metals

MDPI

Review

All-*d*-Metal Heusler Alloys: A Review

Tarek Bachagha [1,2,*] and Joan-Josep Suñol [2,*]

[1] Physics Department, International Center of Quantum and Molecular Structures, Shanghai University, Shanghai 200444, China
[2] Physics Department, Campus Montilivi s/n, Universitat de Girona, 17071 Girona, Spain
* Correspondence: bachagha@shu.edu.cn (T.B.); joanjosep.sunyol@udg.edu (J.-J.S.)

Abstract: Heusler alloy research has increased considerably in recent years. This is mostly due to their strong desire to develop future smart device applications. However, many limiting variables remain for researchers to overcome in order to enhance their functional properties. The poor mechanical properties of these alloys restrict their use as solid-state cooling materials in magnetic refrigeration devices. A promising strategy, resulting in novel compounds with better mechanical properties and substantial magnetocaloric effects, is favoring the *d*–*d* hybridization with transition-metal elements to replace *p*–*d* hybridization. The term given to these materials is "all-*d*-metal". In light of recent experimental results of the magnetocaloric effect and the increased mechanical characteristics in these alloys (with complex crystallographic behavior due to off-stoichiometry and disorder), a review of this advanced functional behavior is offered. Moreover, the impact of the substitution of transition metal for the *p*-group to increase mechanical ductility and considerable magnetocaloric effects has also been addressed. These Heusler alloys are a potential new class of materials for technological applications because of their optimum functional behavior. Finally, we highlighted the potential challenges and unsolved issues in order to guide future studies on this topic.

Keywords: Heusler alloys; hybridization; magnetocaloric effect; magnetic refrigeration

check for updates

Citation: Bachagha, T.; Suñol, J.-J. All-*d*-Metal Heusler Alloys: A Review. *Metals* **2023**, *13*, 111. https://doi.org/10.3390/met13010111

Received: 23 November 2022
Revised: 19 December 2022
Accepted: 29 December 2022
Published: 5 January 2023

Copyright: © 2023 by the authors. Licensee MDPI, Basel, Switzerland. This article is an open access article distributed under the terms and conditions of the Creative Commons Attribution (CC BY) license (https://creativecommons.org/licenses/by/4.0/).

1. Introduction

Most research funding organizations across the globe prioritize energy efficiency and sustainability, and these issues are often discussed in the media. According to statistics from the Lawrence Livermore National Laboratory, the expected US energy consumption until 2021 corresponds to rejected energy was to be 61%, while only 39% was used in energy services. Other developed countries have similar statistics, such as the United Kingdom and Spain, where 63% rejected energy was detected in 2011. These findings demonstrate the need to focus on the primary energy source and avoid dependency on non-renewable energy sources, as well as devoting major research resources to improving energy conversion efficiency. Most renewable energy sources must be converted, in particular, into electricity before being used, with 67% of the conversion process resulting in lost energy in the United States in 2015 [1]. In many cases, magnetic materials play a vital role in the conversion of energy into electricity. This is a driving force behind the development of magnetic materials for energy applications [2]. Air conditioning and refrigeration consume a significant amount of electricity in both the residential and industrial sectors, with quantities varying from country to country due to climatic differences. In fact, specific effects appear when ferromagnetic shape memory alloys (FSMAs) are subjected to external magnetic fields (magnetocaloric (MCE)), hydrostatic pressure (barocaloric (BCE)), and uniaxial stress (elastocaloric (eCE)), this technology is dependent on thermal processes [3–7]. Due to its important role in improving refrigeration system functionality, exploring good materials based on caloric impacts has progressively grown to be a hot research topic. The exceptional multi-magnetofunctional features of Ni−Mn-based Heusler alloys, connected to their tightly coupled ferromagnetic (FM) martensitic transition (MT) around transition

temperature (T_t), have received growing interest. Moreover, Ni−Mn-based alloys generally display the first-order phase transition (FOPT) related to the magnetic transition because of the strong coupling between lattice structure transition and magnetism [8]. Furthermore, a significant MCE is caused by a rapid shift in magnetization from a weak-magnetic to a ferromagnetic (FM) state when the magnetic field is applied or removed. Therefore, during MT and under uniaxial stress, the eCE would be created by the FOPT. Due to the coexistence of MCE and eCE, these alloys are being evaluated as potential prospects for industrial uses. The Ni–Mn–Ga [9], Ni–Mn–Ga–Co [10], Co–Ni–Al [11], Ni–Mn–Sn–Cu [12], and Ni–Co–Mn–Sn [13] shape memory alloys have been examined as exhibit both properties. Because of their excellent magnetic properties and tunable MT temperatures, Ni–Mn-based alloys have been regarded as improved alloys among these noted [14]. In addition, the brittleness of most of these alloys restricts their applications and causes cracking under repetitive stress cycling [15]. Moreover, to reduce the hysteresis behavior associated with MT and improve the mechanical performance, several methods, such as introducing a second phase into grain boundaries, alloying with additional elements, and micro-alloying with boron, are proposed [16–18]. However, the covalent character of this orbital has recently been linked to the poor mechanical performance of Heusler alloys, a disadvantage that limits practical use [19]. Due to their mechanical response, Heusler alloys' useful life as cooling materials and/or mechanical actuators is reduced, which causes structural fatigue when subjected to repeated thermo-mechanical/magnetic cycles. It is well-known that intrinsic brittleness is one of the largest and most pressing concerns to be solved in terms of appropriateness for technology applications [20].

Several approaches have been employed to restrict the macroscopic effects of the intrinsic brittle nature of these alloys, as briefly discussed in reference [21]. However, significant findings of a distinct class of Heusler alloys generated by substituting the *p*-group atom with a third transition metal, i.e., alloys made entirely of transition metal elements, have been found in recent years. In these alloys, considerable *p–d* hybridization among the elements is replaced by *d–d* hybridization, resulting in increased mechanical properties [19,22] associated with the MT and intense MCEs.

This review examines the basic and functional features of full Heusler alloys, with a particular focus on the impact of *p–d* orbital hybridization. Following that, we discuss the basic and functional features of all-*d*-metal Heusler alloys, with a focus on the effect of *d–d* orbital hybridization. Then, we examine some of the most current research on these unique families. Finally, we provide an outlook on the issue, as well as some perspectives for future research.

2. Heusler Alloys

2.1. Composition

Heusler alloys are magnetic intermetallic with face-centered cubic structure and composition of XYZ (half-Heusler) or X_2YZ (full-Heusler), where X and Y are transition metals, and Z is in the *p*-group [23]. In a few cases, the Y atom can be replaced by alkaline earth metal or rare earth (lanthanide family) [24]. In the molecular formula, the transition metal element with the most atoms is placed first, followed by the *p*-group atom.

2.2. Crystalline Structure

Full Heusler alloys crystallize in a face-centered cubic structure that belongs to the *Fm3m* space group and includes Cu_2MnAl as the prototype structure at room temperature (RT). This crystallographic structure is referred known as $L2_1$. Heusler alloys X_2YZ typically have an ordered cubic structure. The four Wyckoff positions in the lattice are A (0, 0, 0), B ($\frac{1}{4}$, $\frac{1}{4}$, $\frac{1}{4}$), C ($\frac{1}{2}$, $\frac{1}{2}$, $\frac{1}{2}$), and D ($\frac{3}{4}$, $\frac{3}{4}$, $\frac{3}{4}$). These alloys obey the site preference rules where X and Y are *d*-group atoms, and Z is a *p*-group atom [25], which determines the site occupancy for X_2YZ stoichiometry, as shown in Figure 1. De Paula et al. [26] and Burch et al. [27] proposed empirical site occupancy rules decades ago, indicating that the atoms of the *p*-group prefer (D) sites, whereas the (A, C) sites are occupied by the transition

metals with more valence electrons, resulting in the highly ordered $L2_1$ structure. According to these rules, the (B) site was occupied by the other transition metal. Usually, the site preference of different 3*d* elements in Heusler alloys is determined by the number of their valence electrons [28]: elements with more valence electrons tend to enter the (A, C) sites and form a Cu_2MnAl type of structure, while elements with fewer electrons prefer the B sites and form a Hg_2CuTi type of structure; the main group elements usually occupy the D sites. We draw attention to the fact that these principles explain why individual atoms' electronic valences are *p* or *d* [29]. Another possible order is that an inverse Heusler structure is created when the valence of the Y atom is larger than that of the X atom, with the Y atom occupying the (A) site and one of the X atoms being reallocated to the (B) site. A multitude of disordered alternate forms is associated with this $L2_1$ structure. The *XA* inverse Heusler structure is a cubic structure that belongs to the space group *F43m* and has $CuHg_2Ti$ as its prototype structure. It is a common occurrence in Mn_2-based compounds.

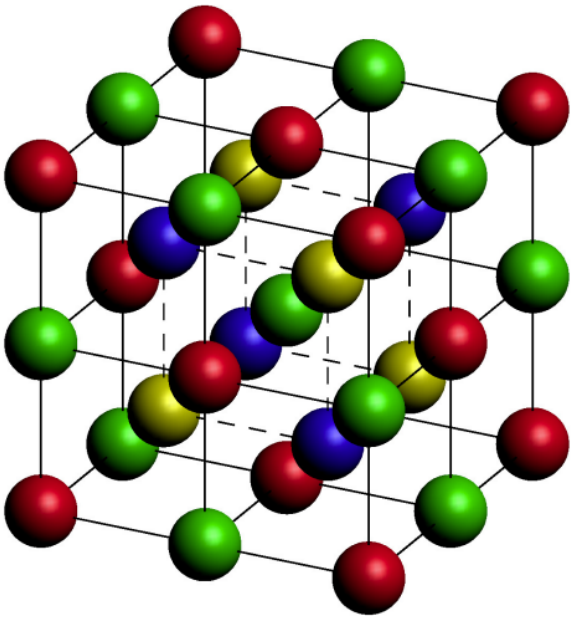


Figure 1. Crystallographic structure of X_2YZ Heusler alloys is shown in this diagram. Blue (A sites), green (B sites), yellow (C sites), and red (D sites).

For the purposes of this review, it is useful to present two types of distinct disordered structures. The *B2*-type disorder is created when the Y and Z atoms indistinctly occupy B and D sites. Thus, in the figure, green and red sites are equivalent, resulting in a symmetry-reduced cubic structure with the space group *Pm3m*.

Finally, a completely disordered structure named *A2*-type disordered structure can arise when all X, Y, and Z sites are equivalent, resulting in a body-centered cubic lattice with decreased symmetry and space group *Im3m*. Thus, in the crystallographic phase, a unique color can be used to draw all atoms. By way of summary, Table 1 shows the sites (A, B, C, and/or D) of the atoms of X, Y, and Z (for a stoichiometric composition).

Table 1. Sites associated withX, Y, and Z atoms for the different austenitic phases of Heusler-type stoichiometry alloys.

Structure	X Atoms (Sites)	Y Atoms (Sites)	Z Atoms (Sites)
$L2_1$	A, C	B	D
Inverse *XA*	B, C	A	D
Disordered *B2*	A, C	B, D	B, D
Disordered *A2*	A, B, C, D	A, B, C, D	A, B, C, D

2.3. Influence of p–d Hybridization

The creation of hybrid orbitals may be understood in light of traditional molecular orbital theory, which is responsible for defining the various forms of chemical bonding in solids [30]. The macroscopic mechanical behavior of materials is described by $C_{i,j}$ elastic constants [31], which are directly dependent on the atomic chemical bonds. The correlation between the degree of *p–d* hybridization and mechanical properties of Ni_2MnZ (Z = Al, Ga, In, Si, Ge, and Sn) has been recently investigated via first-principle calculations by Yan et al. [32]. This study illustrates how the choice of the *p*-group atom strongly affects the three elastic constants (C11, C12, and C44) characteristic of a cubic lattice. Typical X_2MnZ Heusler specimens show a distinct structural phase transition, resulting in multifunctional characteristics. Winterlik et al. [33] reported the electronic structure calculations for Heusler alloys to investigate candidates for superconductivity and identified several Ni_2-based Heusler alloys that become superconducting in the low-temperature region. The superconductivity aspect appears in the system $(Eu_{1-x}Pr_x)BCO$ [34]. As part of this MT, the material transitions from a high-temperature austenite phase with cubic symmetry to a low-temperature martensitic phase with decreasing symmetry. The fact that the atoms actively rearrange themselves using a shear-like process while keeping their relative positions is its most distinctive feature [35]. When it comes to controlling the MT temperature range, the level of the *p–d* orbital hybridization process between the *p* states of Z atoms and the *d* states of X atoms is also significant [36–38]. Moreover, the enhancement of mechanical properties of all-*d*-metal full Heusler alloys is the main achievement caused by the suppression of *p–d* hybridization, as depicted in Table 2. The lower values of Young's elastic modulus exhibited by all-*d*-metal Heusler in comparison to conventional ones are related to its higher ductility since it is a quantitative parameter of the resistance to elastic deformation upon mechanical load [39–43].

Table 2. Young's elastic modulus E for some representative conventional (*p–d*) and all-*d*-metal (*d–d*) Heusler alloys.

Composition	Ni_2MnAl	$Ni_{1.48}Co_{0.52}Mn_{1.4}Ti_{0.6}$	Ni_2MnGa
Type	*p–d*	*d–d*	*p–d*
E (Gpa)	192.00	54.81	124.61
Refs.	[39]	[40]	[41]

From a practical standpoint, stoichiometric variation or partial atomic replacement can be used to tailor MT for specific applications. Both situations have a different number of electrons available for this interaction. The valence electron concentration per atom (*e/a*) measures this distinct property and is expressed as [39]:

$$(e/a) = \frac{1}{2}[N_X f_X + N_Y f_Y + N_Z f_Z]/100, \quad (1)$$

where N_X, N_Y, and N_Z are the number of valence electrons of each element, and f_X, f_Y, and f_Z stand for their corresponding atomic percentages.

A linear dependency of MT versus the (e/a) ratio for many common X_2MnZ Heusler compounds is usually found [22]. Likewise, the austenite (AS) to martensite (MS) structural transformation can be accompanied by the ferromagnetic (FM) to paramagnetic (PM) magnetic transformation. Depending on alloy and composition, this magnetic transformation can appear in the austenite or in the martensitic regions. Thus, all the combinations are possible: AS-FM, AS-PM, MS-FM, and MS-PM. Figure 2 shows a temperature transformation diagram. The slope of the martensitic start temperature (Ms) is influenced by choice of the *p*-element. Obviously, some of these alloys present another magnetic behavior as supermagnetism or spin glass [40].

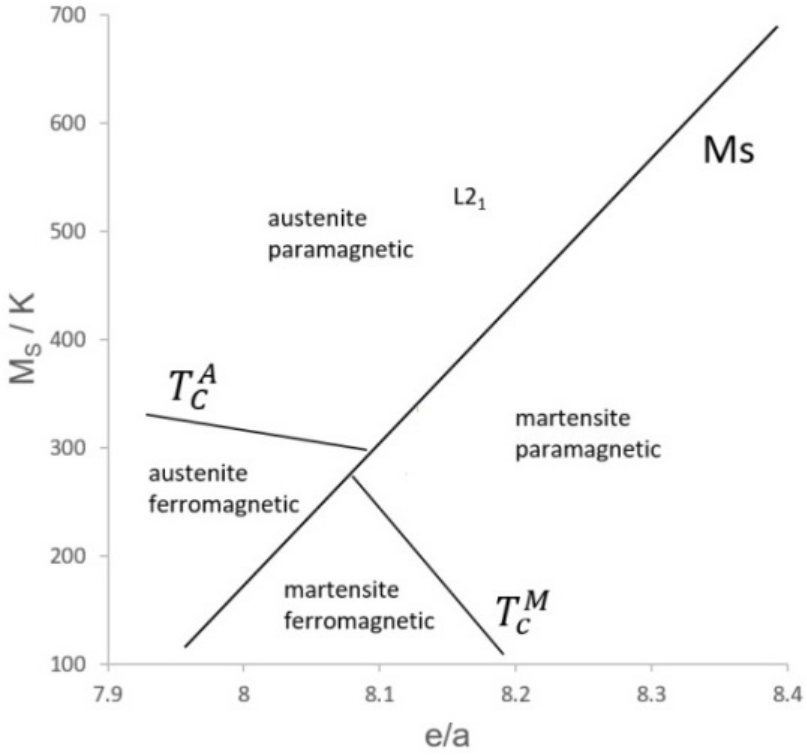


Figure 2. Temperature (martensitic start Ms) transformation diagram topic of Heusler alloys (Reprinted with permission from ref. [44]. Copyright 2022 MDPI).

2.4. MCE in Heusler Alloys

In 1983, Wachtel et al. [45] and Maeda et al. [46] produced the first studies on MCE of Heusler $Ni_2(Mn_{1-x}M_x)Sn$ with M = V and Nb(x = 0.1, 0.2, 0.3 and 0.4), $Mn_{3\text{-}y\text{-}z}Cr_yAlC_{1+z}$ (z = 0.1 and y = 0, 0.06, 0.15 and 0.26), and (y = 0 and z = −0.16, −0.08, 0 and 0.1) alloys. They discovered that Curie temperature (T_C) values drop linearly from room temperature (RT) to around 200 K, and $M_s$alsodecreases linearly. The biggest maximum values of magnetic entropy change (ΔS_M) found in the system at x = 0.1 to 0.2 and in the latter one at y = 0 and z = 0.9 are roughly half of Gd, while $(\Delta S_M)_{Max}$ steadily declines with increasing x or y. Later, in 2000, at moderate fields (ΔS_M = +4 $Jkg^{-1}K^{-1}$ at 0.9 T), Hu et al. [47] observed an inverse MCE attributed to MT (thermal hysteresis 10 K. Due to the substantial uniaxial magneto-crystalline anisotropy of the martensitic phase, inverse MCE arises when both phases are FM, and the high-temperature phase (austenite) has a stronger magnetization than the low-temperature phase (martensite) at low fields [48]. However, for fields larger than 1 T, inverse MCE is replaced with direct MCE [49,50]. A giant MCE [51] was discovered in the compositional area where the magnetostructural transition occurs. Zhou et al. [52,53] studied magnetic and structural transitions, as well as MCE, in Ni_2MnGa alloys. Because Ni-rich alloys have a lower T_C than Mn-rich alloys, their MT is closer to RT. By using neutron diffraction on Ni_2MnGa and $Ni_{1.75}Mn_{1.25}Ga$ systems, Singh et al. [54] recently showed that the inverse MCE is caused by the antiferromagnetic (AFM) contact between Mn atoms at in-equivalent sites. Figure 3 depicts the ΔS_M values' field dependency in two examples: adapted from reference Ni_2MnGa and $Ni_2MnGa_{0.95}Sn_{0.05}$ [55].

Sasso et al. [56], whose results are consistent with those of Khovaylo et al. [57], who attributed differences in field-applied and field-removed curves to magnetostructural hysteresis, also highlighted MCE's historical dependence on the field and thermal sequence. Porcary et al. [58] established the convergence of direct and indirect methodologies in the analysis of Ni(Co)–Mn–Ga alloy. There are various arguments against using Heusler alloys as magnetic refrigerants, including the irreversible nature of the magnetic field-driven MT and the considerable hysteresis found [54]. As a result, researchers in MCE for Heusler alloys are presently focusing their efforts on removing hysteresis. Inverse giant MCE in

$Ni_{50}Mn_{37}Sn_{13}$ was reported by Krenke et al. [59] in 2005, while Han et al. [60] reported inverse giant MCE in In-containing Heusler alloys in 2006. Later, in 2007, Khan et al. [61] and Du et al. [62] indicated a good correlation for $Ni_2Mn_{1+x}Z_{1-x}$ (Z = In, Sn, and Sb) and $Ni_{50-x}Mn_{37}Sb_{13}$ alloys close to stoichiometric composition (x = 0.3) showing a cubic $L2_1$ austenitic phase and a typical FM/PM magnetic transition preserving this austenitic phase. However, alloys with a higher divergence from 2:1:1 stoichiometry show MT. In contrast to Ga-containing Heusler alloys, AFM coupling between Mn atoms is enhanced (martensitic state) in these alloys, resulting in a metamagnetic transformation from AFM to FM, which may be adjusted to be a meta-magneto-structural transition from AFM to FM austenitic phase. It has been proposed that the existence of both (direct and inverse) MCE is a mechanism for increased refrigeration cycle performance [63].

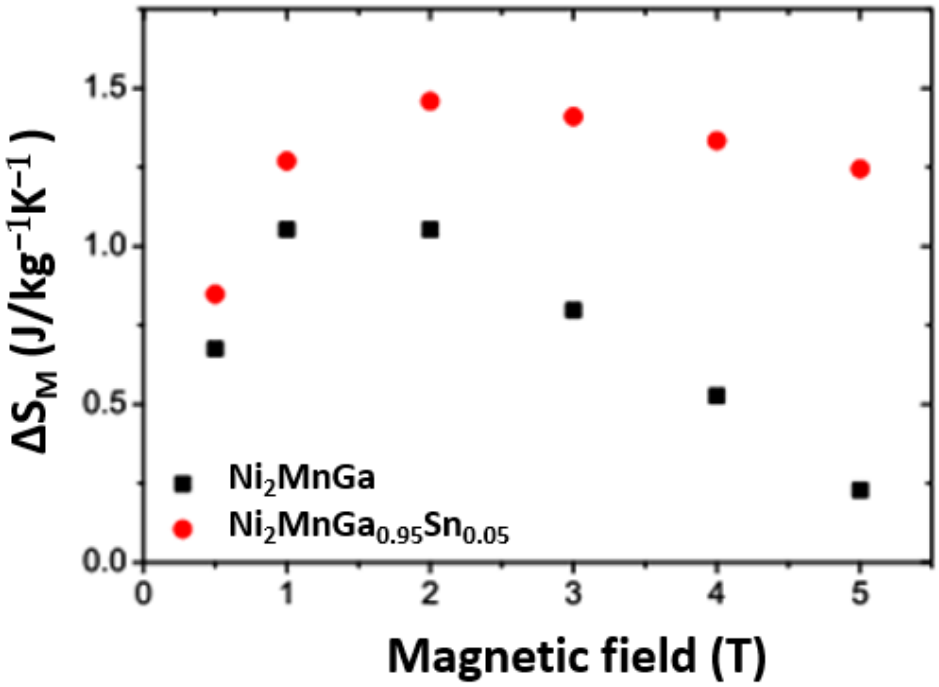


Figure 3. Field dependence of ΔS_M for $Ni_2MnGa_{1-x}Sn_x$ (x = 0 and 0.05) alloys. Reproduced from reference [55]. Copyright 2012 Elsevier.

Due toits MCE, several Heusler alloy families have been studied. Temperatures surrounding the second-order phase transition (SOPT) of Ni–Mn–Ge have been observed [64], with T_C decreasing as the Ni/Mn ratio increases. Ni–Fe–Ga [65], Ni–(Fe,Co)–Ga [66], and Co–Ni–Ga [67] are examples of Mn-free systems discovered in the literature. Due to its higher ductility, Ni–Fe–Ga has been advocated as a superior MCE material than Ni–Mn–Ga. Its MCE effect is field dependent, similar to Ni–Mn–Ga, and at low fields, it switches from inverse to conventional MCE. Co helps to align the Curie temperatures of martensite and austenite phases with the transition temperature of MT by shifting to higher levels. Moderate MCE values were reported: ΔS_M (5 T) = 2.4 Jkg^{-1}K^{-1} at 360 K [63]. On the other hand, the higher MCE values of $Co_{50}Ni_{22}Ga_{28}$ alloy were reported: ΔS_M (5 T) = 10.5 Jkg^{-1}K^{-1} at 313.5 K, which was attributed to the MT between FM martensite and FM austenite [64]. On the other hand, its sharp ΔS_M(T) curves are full width at half maximum (FWHM < 2 K), and the considerable thermal hysteresis of the MT (20 K) must be taken into account. Vivas et al. [68] studied the effects of the number of valence electrons on the MCE of half-metal $Fe_2MnSi(Ga)$ alloys and found a phenomenological linear relationship between ΔS_M and this parameter. In summary, Figure 4 shows the ΔS_M values at 5 T as a function of the transition temperatures of various Heusler alloys.

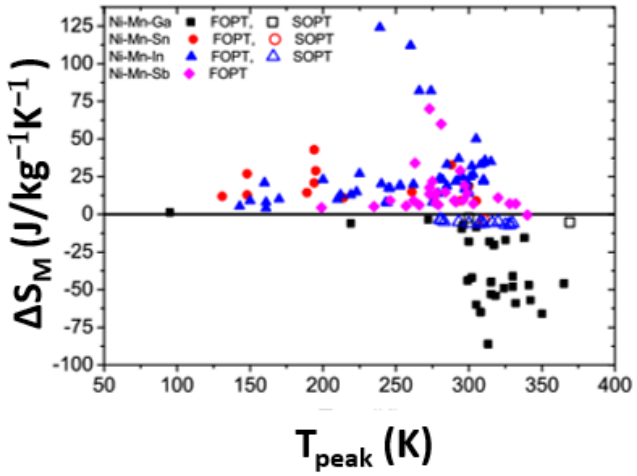


Figure 4. ΔS_M values for several Heusler alloys as a function of peak temperatures (T_{peak}) at 5 T. Reprinted with the permission from refs. [65–68]. Copyrights 2008, 2009 and 2016 Elsevier.

3. All-*d*-Metal Heusler Alloys

3.1. Background of These Kinds of Alloys

Recently, Wei et al. [22] suggested the notion of an all-*d*-metal Heusler based on *d*–*d* orbital hybridization. The authors of this seminal work established the term "all-*d*-metal" after discovering that the Heusler phase could be formed without the *p*-group atom. Experiments on the crystal structure of Zn_2AuAg and Zn_2CuAg compounds [69,70] may be traced all the way back to the 1960s. Both compounds have $L2_1$ organized and *B2* disordered structures, according to these ancient publications. The Zn_2AuAg, in particular, shows a *B2* to $L2_1$ order-disorder transition, as evidenced by changes in structural order characteristics. On the other hand, their applications as FSMAs are limited due to the absence of FM ordering in these alloys, and no further research on these alloys has been conducted as far as we know. Both alloys now belong within the category of Heusler alloys since the notion of all-*d*-metal Heusler is widely known.

3.2. Crystalline Structure

In the recently found $Ni_2Mn_{2-y}Ti_y$ and $Ni_{2-y}Mn_2Ti_y$ systems, Ti atoms have the fewest valence electrons ($3d^24s^2$) compared to Ni ($3d^84s^2$) and Mn ($3d^54s^2$), and Wei et al. [22] predicted that Ti would occupy the D site. Both systems crystallize in a *B2*-type disordered structure, with the Mn excess atoms sharing the D site with Ti atoms in the $Ni_2Mn_{2-y}Ti_y$ system, resulting in a strong AFM coupling due to the Mn(B)–Mn(D) interaction (Figure 5). The main difference with conventional Heusler alloys is the competence between the $L2_1$ and the inverse *XA* phases.

The $Ni_{2-x}Co_xMn_{1.4}Ti_{0.6}$ quaternary series was discovered by Wei et al. [19], who employed the strategy of introducing Co atoms at Ni sites to impose FM long-range ordering on the Ni–Mn–Ti system, resulting in the first FSMAs among all-*d*-metal Heusler alloys. Partially replacing Co atoms in Ni_2MnZ systems has previously been investigated [71], resulting in a strong local Mn(B)–Co(A/C)–Mn(D) exchange coupling with FM ordering [72], overcoming the Mn(B)–Mn(D) AFM coupling inherent in the *B2*-type disordered lattice. Moreover, some experimental results observed that strong ferromagnetism provides direct evidence of this probable atomic configuration and of the ferromagnetic activation effect in the Ni(Co,Fe)–Mn–Ti all-*d*-metal Heusler alloys. For example, in $Ni_{50-x}Co_xMn_{35}Ti_{15}$ alloys, Co atoms that have been substituted for Ni atoms will also share the (A,C) sites with Ni atoms, leaving Mn and Ti with fewer valence electrons at the B/D sites. With the aid of the strong FM exchange interactions between nearest-neighbor Co-Mn atoms, the original AFM exchange coupling between Mn-Mn atoms in Ni-Mn-Ti alloys is converted into FM one, resulting in parallel alignment of the Mn-Co-Mn moments [19]. This phenomenon is known as the "ferromagnetic activation effect of the Co atom" [72]. FM ordering in

$Ni_{2-x}Fe_xMn_{1.4}Ti_{0.6}$ alloys [73], in which Fe substitutes Co in the exchange coupling, is generated via a similar mechanism. Co ($3d^74s^2$) and Fe ($3d^64s^2$) atoms are considered to share the (A/C) sites with Ni ($3d^84s^2$) atoms in both series since their valence numbers are greater than those of Mn and Ti. Feng [74] used theoretical calculations on the X_2MnTi (X = Pt and Pd) series to study the impact of Ti as a *p*-group atom replacement. The findings show that the $L2_1$ crystallographic structure is energetically stable for both compositions, with high valence Pd ($4d^85s^2$) and Pt ($5d^86s^2$) filling the (A/C) sites and Mn ($3d^54s^2$) occupy the (B) site, respectively. Ti prefers to remain in the D site. Han et al. [75] developed research for all-*d*-metal Heusler alloys $X_{2-x}Mn_{1+x}V$ (X = Pd, Ni, Pt, Ag, Au, Ir, Co; x = 1, 0). They looked at the atomic occupancy of these alloys in the cubic phase and discovered that the well-known site preference criterion does not apply to all of them. Han et al. [76,77] and Wang et al. [78] studied other Zinc-based all-*d*-metal Heusler ZnCdTMn combinations by theoretical calculations on the Zn_2YMn series. As a result of its complete 3*d* occupied state, the Zn atoms behave as a major group element, and Zn atoms prefer to occupy the D site rather than replacing Pd atoms at site A. The phenomenon of this process is the whole 3*d* shell of the Zn atom.

In Figure 5, as the content of Ti was usually lower than 25 at.%, some Mn atoms are located on D sites by substituting Ti atoms. However, the martensitic crystallographic structure can be more complex, including modulation, as shown in Figure 6.

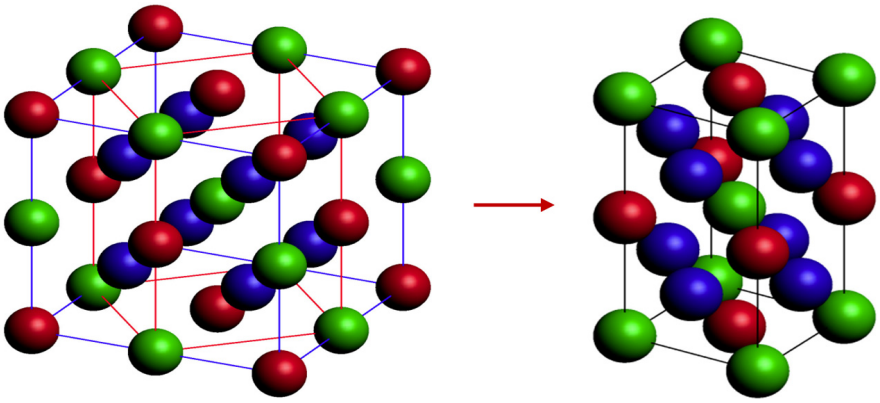


Figure 5. Schema of the $L2_1$ Heusler crystallographic structure (**left**) indicating with red lines the cell of the $L1_0$ tetragonal martensite (**right**) for stoichiometric $Ni_{50}Mn_{25}Ti_{25}$ alloy.

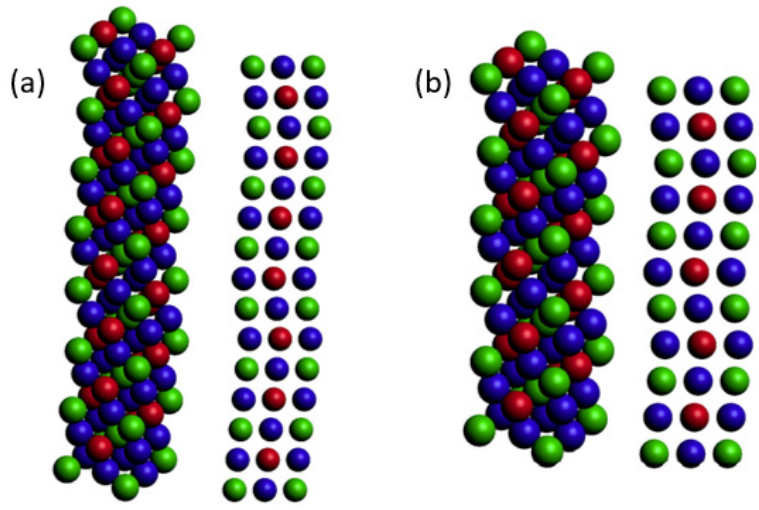


Figure 6. (**a**) Cell of the seven-layer modulated martensite phase (14M) of an arbitrary composition sample seen in 3D and laterally. (**b**) Cell of the five-layer modulated martensite phase (10M) of an arbitrary composition sample seen in 3D and laterally (generated with MAUD-free software, version 2.08, Luca Lutterotti, Trento, Italy).

3.3. Influence of d–d Hybridization

Theoretical calculations revealed that stoichiometric Ni_2MnTi displays mechanical properties superior to those of conventional Heusler systems. Yan et al. [79] later discovered that the $Ni_{2.0}Mn_{1.27}Ti_{0.73}$ composition has a significant eCE (under 600 MPa of uniaxial stress, adiabatic temperature change $\Delta T_{ad} = -20.4$ K). Many Ni–Mn-based systems, such as $Ni_{1.80}Mn_{1.76}Sn_{0.44}$ ($\Delta T_{ad} = -11.6$ K unloading 600 MPa of uniaxial stress) [80] and $Ni_{2.0}Mn_{1.11}Ga_{0.89}$ (unloading 100 MPa of uniaxial stress, $\Delta T_{ad} = -6.1$ K) [81], have lower values. Changing the chemical bonding character of the $Ni_{2.0}Mn_{1.27}Ti_{0.73}$ all-*d*-metal Heusler alloy by substituting high *p–d* hybridization with somewhat weaker *d–d* hybridization among transition metals increases its ductility, according to further examination of the electron localization function. Pugh's ratio [82] is a popular metric for determining solid ductility. It is defined as the ratio of the bulk modulus B to the shear modulus G of a material. Values greater than 1.75 indicate ductile behavior. For different X_2MnZ compositions, Figure 7 illustrates Pugh's ratio as a function of Cauchy pressure, a parameter that describes the dominant kind of chemical bonding. We see that Ni_2MnTi is more ductile than Ni_2MnGa [83] and Ni_2MnIn [84], two of the most promising FSMAs among Heusler systems, according to our results. Furthermore, Ni_2MnTi [85] also has the highest Cauchy pressure, indicating that chemical bandings are weakly covalent. As a consequence, reducing covalent *p–d* hybridization in Ni_2MnZ Heusler alloys is connected to enhanced ductility.

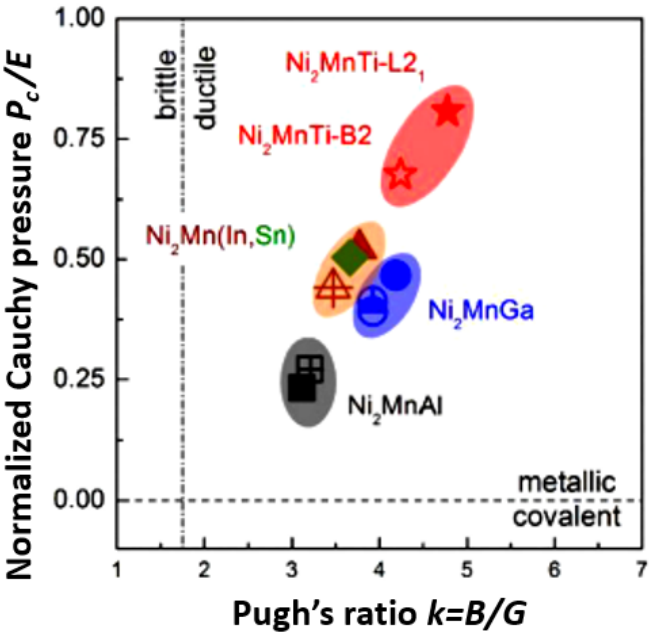


Figure 7. Ductile-brittle diagram of some conventional Ni–Mn–Z (Z = Ga, Al, In and Sn) and stoichiometric Ni_2MnTi alloys. The horizontal dashed and the vertical dashed dot lines indicate Pettifor's and Pugh's brittleness–ductility criteria, respectively. The inhibition of covalent *p–d* hybridization obtained by removing the *p*-group atom is supported by this result. Reproduced with permission from ref. [79]. Copyright 2019 Elsevier.

3.4. MCE in All-d-Metal Heusler Alloys

Until recently, only a few investigations have focused on Heusler alloys of this type. Wei et al. [22] recently discussed the creation of all-*d*-metal alloys that exclusively include 3*d* transition metal components. They found that adding Ti to Ni–Mn aids in the *B2* phase creation and stability. Cong et al. [6] achieved a massive elastocaloric impact in Ni–Mn–Ti alloys, with a $\Delta T_{ad} = 31.5$ K and $\Delta S_M = 45$ Jkg^{-1}K^{-1}, at a pressure of 700 MPa. Yan et al. [77] also discovered that the bulk $Ni_{50}Mn_{31.75}Ti_{18.25}$ alloy has outstanding mechanical characteristics, with a stress of 1.1 GPa and a convincing compressive strain of 13%, respectively. Despite its exceptional elastocaloric sway, the Ni–Mn–Ti combination has a modest MCE

when compared to Heusler alloys. The absence of magnetic contrast between the austenite and martensite phases is largely responsible for this. Yan et al. [79] examined the austenite phase's antiferromagnetic condition in Ni–Mn–Ti alloys. As a result, some thought has been given to doping the elements to improve the magnetocaloric impact. Furthermore, according to Wei et al. [19], cobalt doping in the $Ni_{50}Mn_{35}Ti_{15}$ alloy affects the transition from AFM to FM in the austenite phase. They created the Mn–Co–Mn configuration by replacing Co for Ni sites in the austenite phase, resulting in the ferromagnetic activation effect. Additionally, the AFM state of austenite in Ni–Mn–Ti alloys was confirmed by Yan et al. [79] and Wei et al. [19]. Therefore, some researchers have attempted to improve its MCE by means of doping elements. Li et al. [86] indicated that under a magnetic field of 3 T, Fe and Co doping in the Ni–Mn–Ti alloy could produce the refrigeration capacity (RC) of 79.5 Jkg^{-1} and ΔS_M of 8.4 $Jkg^{-1}K^{-1}$. In addition, taking into account the magnetostructural coupling in the $Ni_{2-x}Fe_xMnTi$ [81] and Ni–Co–Mn–Ti [73] Heusler alloys, a giant MCE was observed. Recently, Aznar et al. [87,88] revealed the B-doped $Ni_{50}Mn_{31.5}Ti_{18.5}$ all-*d*-metal Heusler alloy. These alloys created an excellent BCE with an RC up to 1100 Jkg^{-1} and ΔS_M of 74 $Jkg^{-1}K^{-1}$ under the pressure of 3.8 kbar, undergoing MT with an enormous volume change (ΔV) in its PM. Due to the eCE and MCE coexisting near RT, these alloys must be candidates for magnetic refrigeration.

3.5. Perspectives

Recently, experimental efforts targeted at increasing the MCE of all-*d*-metal Heusler alloys are worth emphasizing. One option is to add more elements to analyze multicomponent specimens and the effect of the combination of four or fifth elements in the functional response in a similar pathway to the applied to conventional Heusler alloys. Taubel et al. [89] revealed that an ideal annealing technique sharpened the phase transformation in the quaternary $Ni_{2-x}Co_xMn_{2-y}Ti_y$ series, while the Co content governs the transition's sensitivity to the external magnetic field. The direct MCE is particularly strong in the $Ni_{1.40}Co_{0.60}Mn_{1.48}Ti_{0.25}$ Heusler alloy (ΔT = 4.0 K and $\Delta S_{iso} = -20.0$ $Jkg^{-1}K^{-1}$ under an applied magnetic field of 20 kOe). Li and coworkers [90] made a significant addition to the field by investigating the $Ni_{1.4}Co_{0.6-x}Fe_xMn_{1.4}Ti_{0.6}$ series experimentally. The partial replacement of Fe atoms with Co atoms decreases the *d*–*d* hybridizations, in this case, changing the Curie temperature and MT temperatures of the system. The maximum direct MCE value ($\Delta S_{iso} = -20.0$ $Jkg^{-1}K^{-1}$ under a field of 50 kOe) was found for the x = 0.024 composition. By applying hydrostatic pressure (0.35 GPa), the functional response is improved, achieving values of $\Delta S_{iso} = -24.20$ $Jkg^{-1}K^{-1}$ and RC = 347.26 JK^{-1} (under a field of 50kOe) [85]. Because this system has both direct and inverse MCE, both demagnetization and magnetization processes may be investigated for solid-state refrigeration.

It should be remarked that these materials are also under study for applications such as catalysis with chemically diverse surface configurations [91]. These materials can also have high magnetoresistance [92] and spintronic properties [93].

We advocate focusing future research on the atomic site occupancy rules of these kinds of alloys. First principles and density functional theory (DFT) studies will be useful in understanding atomic site influence on the total magnetic moment per formula unit [89–94]. It is known that a large reversible magnetocaloric effect and high magnetoresistance were achieved by improving the crystallographic compatibility between the austenitic and martensitic phases [95]. Likewise, the influence of *d*–*d* hybridizations on atomic ordering may be shown by evaluating structural and magnetic properties when the quantity of the *p*-atom group decreases. Furthermore, the impact of thermal annealing, applied pressure as well as several synthesis methods on the creation of the $L2_1$ phase should be further investigated. Finally, because of the increased mechanical ductility and high induced strain values observed, the shape memory impact of ternary $Ni_{2x}Mn_{1+x}Ti_x$ and $Mn_{2x}Ni_{1+x}Ti_x$ series should be further investigated.

4. Conclusions

By removing the *p*-group atom from the X_2YZ composition, novel functional all-*d*-metal Heusler alloys are developed. These findings contribute to our knowledge of the role of orbital hybridization in the fundamental and functional features of X_2YZ Heusler alloys. According to the current study, despite the lack of a *p*-group atom, the martensitic transition with adjustable MT by chemical composition occurs. Finally, substituting a transition metal for the *p*-group enhances mechanical ductility and results in considerable reversible MCE. The suppression of *p*–*d* hybridization and the growth of *d*–*d* hybridizations is the key physical process that combines remarkable mechanical features with huge MCE. Because of their optimal functional behavior, these alloys are a possible new class of materials for technological applications. We advocate focusing future research on the atomic site occupancy rules of these kinds of alloys. The influence of *d*–*d* hybridizations on atomic ordering may be shown by evaluating structural and magnetic properties when the quantity of the *p*-atom group decreases. Furthermore, the impact of thermal annealing techniques, as well as several synthesis methods on the creation of the $L2_1$ phase, should be further investigated. Finally, because of the increased mechanical ductility and high induced strain values observed, the shape memory impact of ternary $Ni_{2x}Mn_{1+x}Ti_x$ and $Mn_{2x}Ni_{1+x}Ti_x$ series should be further investigated.

Author Contributions: Conceptualization, T.B.; methodology, T.B. and J.-J.S.; writing—original draft preparation, T.B.; writing—review and editing, J.-J.S. and T.B. All authors have read and agreed to the published version of the manuscript.

Funding: This study was funded by the University of Girona PONT2020-01 and Mineco Spain MAT2016-75967-P projects.

Data Availability Statement: Data can be requested from the authors.

Acknowledgments: The authors acknowledge A. Carrillo for the MAUD crystallography images support.

Conflicts of Interest: The authors declare no conflict of interest.

References

1. Laurence Livermore National Laboratory. Energy Flow Charts. Available online: https://flowcharts.llnl.gov/commodities/energy (accessed on 22 November 2022).
2. Gutfleisch, O.; Willard, M.A.; Bruck, E.; Chen, C.H.; Sankar, S.G.; Liu, J.P. Magnetic Materials and Devices for the 21st Century: Stronger, Lighter, and More Energy Efficient. *Adv. Mater.* **2011**, *23*, 821–842. [CrossRef] [PubMed]
3. Wu, Y.F.; Xuan, H.C.; Agarwal, S.; Xu, Y.K.; Zhang, T.; Feng, L.; Li, H.; Han, P.D.; Zhang, C.L.; Wang, D.H.; et al. Large magnetocaloric effect and magnetoresistance in Fe and Co co-doped Ni-Mn-Al Heusler alloys. *Phys. Status Solidi A* **2018**, *215*, 1700843. [CrossRef]
4. Franco, V.; Blázquez, J.S.; Ipus, J.J.; Law, J.Y.; Moreno-Ramírez, L.M.; Conde, A. Magnetocaloric effect: From materials research to refrigeration devices. *Prog. Mater. Sci.* **2018**, *93*, 112–232.
5. Stern-Taulats, E.; Planes, A.; Lloveras, P.; Barrio, M.; Tamarit, J.L.; Pramanick, S.; Majumdar, S.; Yüce, S.; Emre, B.; Frontera, C.; et al. Tailoring barocaloric and magnetocaloric properties in low-hysteresis magnetic shape memory alloys. *Acta Mater.* **2015**, *96*, 324–332. [CrossRef]
6. Cong, D.Y.; Xiong, W.X.; Planes, A.; Ren, Y.; Mañosa, L.; Cao, P.Y.; Nie, Z.H.; Sun, X.M.; Yang, Z.; Hong, X.F.; et al. Colossal elastocaloric effect in ferroelastic Ni-Mn-Ti alloys. *Phys. Rev. Lett.* **2019**, *122*, 255703. [CrossRef] [PubMed]
7. Bonnot, E.; Romero, R.; Mañosa, L.; Vives, E.; Planes, A. Elastocaloric effect associated with the martensitic transition in shape-memory alloys. *Phys. Rev. Lett.* **2008**, *100*, 125901. [CrossRef]
8. Bachaga, T.; Zhang, J.; Khitouni, M.; Sunol, J.J. NiMn-based Heusler magnetic shape memory alloys: A review. *Int. J. Adv. Manuf. Technol.* **2019**, *103*, 2761–2772. [CrossRef]
9. Soto-Parra, D.E.; Vives, E.; González-Alonso, D.; Manosa, L.; Planes, A.; Romero, R.J.; Matutes-Aquino, A.; Ochoa-Gamboa, R.A.; Flores-Zúniga, H. Stress and magnetic field-induced entropy changes in Fe-doped Ni–Mn–Ga shape-memory alloys. *Appl. Phys. Lett.* **2010**, *96*, 071912. [CrossRef]
10. Castillo-Villa, P.O.; Soto-Parra, D.E.; Matutes-Aquino, J.A.; Ochoa-Gamboa, R.A.; Planes, A.; Manosa, L.; González-Alonso, D.; Stipcich, M.; Romero, R.; Ríos-Jara, D.; et al. Caloric effects induced by magnetic and mechanical fields in a $Ni_{50}Mn_{25-x}Ga_{25}Co_x$ magnetic shape memory alloy. *Phys. Rev. B* **2011**, *83*, 174109. [CrossRef]
11. Khan, M.T.; Wang, Y.; Wang, C.; Liao, X.; Yang, S.; Song, X.; Ren, X. Combination of conventional elastocaloric and magnetocaloric effects in a $Co_{37}Ni_{35}Al_{28}$ ferromagnetic shape memory alloy. *Scr. Mater.* **2018**, *146*, 182. [CrossRef]

12. Castillo-Villa, P.O.; Manosa, L.; Planes, A.; Soto-Parra, D.E.; Sánchez-Llamazares, J.L.; Flores-Zúniga, H.; Frontera, C. Elastocaloric and magnetocaloriceffects in Ni-Mn-Sn(Cu) shapememoryalloy. *J. Appl. Phys.* **2013**, *113*, 053506. [CrossRef]
13. Qu, Y.H.; Cong, D.Y.; Li, S.H.; Gui, W.Y.; Nie, Z.H.; Zhang, M.H.; Ren, Y.; Wang, Y.D. Simultaneously achieved large reversible elastocaloric and magnetocaloric effects and their coupling in a magnetic shape memory alloy. *Acta Mater.* **2018**, *151*, 41. [CrossRef]
14. Huang, C.; Wang, Y.; Tang, Z.; Liao, X.; Yang, S.; Song, X. Influence of atomic ordering on elastocaloric and magnetocaloric effects of a Ni–Cu–Mn–Ga ferromagnetic shape memory alloy. *J. Alloys Compd.* **2015**, *630*, 244. [CrossRef]
15. Li, Y.; Sun, W.; Zhao, D.; Xu, H.; Liu, J. An 8 K elastocaloric temperature change induced by 1.3% transformation strain in $Ni_{44}Mn_{45-x}Sn_{11}Cu_x$ alloys. *Scr. Mater.* **2017**, *130*, 278. [CrossRef]
16. Tang, X.; Feng, Y.; Wang, H.; Wang, P. Enhanced elastocaloric effect and cycle stability in B and Cu co-doping Ni-Mn-In polycrystals. *Appl. Phys. Lett.* **2019**, *114*, 033901. [CrossRef]
17. Yang, Z.; Cong, D.Y.; Sun, X.M.; Nie, Z.H.; Wang, Y.D. Enhanced cyclability of elastocaloric effect in boron-microalloyed Ni-Mn-In magnetic shape memory alloys. *Acta Mater.* **2017**, *127*, 33. [CrossRef]
18. Li, Z.B.; Yang, J.J.; Li, D.; Li, Z.Z.; Yang, B.; Yan, H.L.; Sánchez-Valdés, C.F.; Sánchez Llamazares, J.L.; Zhang, Y.D.; Esling, C.; et al. Tuning the reversible magnetocaloric effect in Ni–Mn–In-based alloys through Co and Cu Co-doping. *Adv. Electron. Mater.* **2019**, *5*, 1800845. [CrossRef]
19. Wei, Z.Y.; Liu, E.K.; Chen, J.H.; Li, Y.; Liu, G.D.; Luo, H.Z.; Xi, X.K.; Zhang, H.W.; Wang, W.H.; Wu, G.H. Realization of multifunctional shape memory ferromagnets in all-*d*-metal Heusler phases. *Appl. Phys. Lett.* **2015**, *107*, 022406. [CrossRef]
20. Tusek, J.; Žerovnik, A.; Čebron, M.; Brojan, M.; Žužek, B.; Engelbrecht, K.; Cadelli, A. Elastocaloric effect vs fatigue life: Exploring the durability limits of Ni-Ti plates under pre-strain conditions for elastocaloric cooling. *Acta Mater.* **2018**, *150*, 295–307. [CrossRef]
21. Liu, J.; Zhao, D.; Li, Y. Exploring magnetic elastocaloric materials for solid-state cooling. *Shap. Mem. Superelasticity* **2017**, *3*, 192–198. [CrossRef]
22. Wei, Z.Y.; Liu, E.K.; Li, Y.; Han, X.L.; Du, Z.W.; Luo, H.Z.; Liu, G.D.; Xi, X.K.; Zhang, H.W.; Wang, W.H.; et al. Magnetostructural martensitic transformations with large volume changes and magnetostrains in all-*d*-metal Heusler alloys. *Appl. Phys. Lett.* **2016**, *109*, 071904. [CrossRef]
23. Meinert, M.; Schmalhorst, J.M.; Reiss, G.; Arenholz, E. Ferrimagnetism and disorder of epitaxial $Mn_{2-x}Co_xVAl$ Heusler compound thin films. *J. Phys. D Appl. Phys.* **2011**, *44*, 215003. [CrossRef]
24. Graf, T.; Felser, C.; Parkin, S.S.P. Simple rules for the understanding of Heusler compounds. *Prog. Solid State Chem.* **2011**, *39*, 1–50. [CrossRef]
25. Li, G.J.; Liu, E.K.; Zhang, H.G.; Qian, J.F.; Zhang, H.W.; Chen, J.L.; Wang, W.H.; Wu, G.H. Unusual lattice constant changes and tunable magnetic moment compensation in $Mn_{50-x}Co_{25}Ga_{25+x}$ alloys. *Appl. Phys. Lett.* **2012**, *101*, 102402. [CrossRef]
26. De Paula, V.G.; Reis, M.S. All-*d*-metal full Heusler alloys: A novel class of functional materials. *Chem. Mater.* **2021**, *33*, 5483–5495. [CrossRef]
27. Niculescu, V.; Burch, T.J.; Raj, K.; Budnick, J.I. Properties of Heusler-type materials Fe_2TSi and $FeCo_2Si$. *J. Magn. Magn. Mater.* **1977**, *5*, 60–66. [CrossRef]
28. Kandpal, H.C.; Fecher, G.H.; Felser, C. Calculated electronic and magnetic properties of the half-metallic, transition metal based Heusler compounds. *J. Phys. D Appl. Phys.* **2007**, *40*, 1507. [CrossRef]
29. Ma, L.; Wang, W.H.; Zhen, C.M.; Hou, D.L.; Tang, X.D.; Liu, E.K.; Wu, G.H. Polymorphic magnetization and local ferromagnetic structure in Co-doped Mn_2NiGa alloys. *Phys. Rev. B Condens. Matter Mater. Phys.* **2011**, *84*, 224404. [CrossRef]
30. Pauling, L. The nature of the chemical bond. Application of results obtained from the quantum mechanics and from a theory of paramagnetic susceptibility to the structure of molecules. *J. Am. Chem. Soc.* **1931**, *53*, 1367–1400. [CrossRef]
31. Kittel, C.; McEuen, P. *Introduction to Solid State Physics*; Wiley: New York, NY, USA, 1976; p. 8.
32. Yan, H.L.; Liu, H.X.; Zhang, M.J.; Jia, N.; Bai, J.; Yang, B.; Li, Z.; Zhang, Y.; Esling, C.; Zhao, X.; et al. Electronic origin of the main-group element dependences of elastic moduli in the Ni_2Mn-based magnetic shape memory alloys. *J. Phys. Chem. Solids* **2021**, *148*, 109671. [CrossRef]
33. Winterlik, J.; Fecher, G.H.; Felser, C.; Jourdan, M.; Grube, K.; Hardy, F.; Löhneysen, H.V.; Holman, K.L.; Cava, R.J. Ni-based superconductor: Heusler compound $ZrNi_2Ga$. *Phys. Rev. B* **2008**, *78*, 184506. [CrossRef]
34. Peczkowski, P.; Zachariasz, P.; Jastrzebski, C.; Pietosa, J.; Drzymała, E.; Gondek, Ł. On the Superconductivity Suppression in $Eu_{1-x}Pr_xBa_2Cu_3O_{7-\delta}$. *Materials* **2021**, *14*, 3503. [CrossRef] [PubMed]
35. Khachaturyan, A.G. *Theory of Structural Trans-Formations in Solids*; Courier Corporation: New York, NY, USA, 2013.
36. Roy, S.; Blackburn, E.; Valvidares, S.M.; Fitzsimmons, M.R.; Vogel, S.C.; Khan, M.; Dubenko, I.; Stadler, S.; Ali, N.; Sinha, S.K.; et al. Delocalization and hybridization enhance the magnetocaloric effect in Cu-doped Ni_2MnGa. *Phys. Rev. B Condens. Matter Mater. Phys.* **2009**, *79*, 235127. [CrossRef]
37. Li, G.J.; Liu, E.K.; Zhang, H.G.; Zhang, Y.J.; Xu, G.Z.; Luo, H.Z.; Zhang, H.W.; Wang, W.H.; Wu, G.H. Role of covalent hybridization in the martensitic structure and magnetic properties of shape-memory alloys: The case of $Ni_{50}Mn_{5+x}Ga_{35-x}Cu_{10}$. *Appl. Phys. Lett.* **2013**, *102*, 062407. [CrossRef]
38. Krenke, T.; Moya, X.; Aksoy, S.; Acet, M.; Entel, P.; Mañosa, L.; Planes, A.; Elerman, Y.; Yücel, A.; Wassermann, E.F. Electronic aspects of the martensitic transition in Ni−Mn based Heusler alloys. *J. Magn. Magn. Mater.* **2007**, *310*, 2788–2789. [CrossRef]
39. Yang, S.; Kong, Y.; Du, Y.; Shen, L.; Shen, Y. First-principles prediction of structural, mechanical and magnetic properties in Ni_2MnAl. *Comput. Mater Sci.* **2016**, *123*, 52–58. [CrossRef]

40. Liu, K.; Ma, S.; Ma, C.; Han, X.; Yu, K.; Yang, S.; Zhang, Z.; Song, Y.; Luo, X.; Chen, C.; et al. Martensitic transformation and giant magnetofunctional properties in all-d-metal Ni-Co-Mn-Ti alloy ribbons. *J. Alloys Compd.* **2019**, *790*, 78–92. [CrossRef]
41. Roy, T.; Gruner, M.E.; Entel, P.; Chakrabarti, A. Effect of substitution on elastic stability, electronic structure and magnetic property of Ni−Mn based Heusler alloys: An ab initio comparison. *J. Alloys Compd.* **2015**, *632*, 822–829. [CrossRef]
42. Ahamed Khan, R.; Ghomashchi, R.; Xie, Z.; Chen, L. Ferromagnetic shape memory Heusler materials: Synthesis, microstructure characterization and magneto-structural properties. *Materials* **2018**, *11*, 988. [CrossRef]
43. Suh, B.; Baek, S.J.; Rhee, J.Y. Antisite disorder and super-paramagnetism in Heusler-like Fe_2Val: A ^{51}V and ^{27}Al NMR study. *J. Korean Phys. Soc.* **2006**, *4*, 288–291.
44. Ameur, R.; Chemingui, M.; Bahaga, T.; Escoda, L.; Khitouni, M.; Suñol, J.J. Martensitic transformation and crystalline structure of $Ni_{50}Mn_{50-x}Sn_x$ melt-spun Heusler alloys. *Crystals* **2020**, *10*, 853. [CrossRef]
45. Wachtel, E.; Henninger, F.; Predel, B. Constitution and magnetic-properties of Ni-Mn-Sn alloys-solid and liquid-state. *J. Magn. Magn. Mater.* **1983**, *38*, 305–315. [CrossRef]
46. Maeda, H.; Sato, M.; Uehara, M. Dawn of research on magnetic refrigeration materials at the National Institute for Materials Research, Science and Technology Agency. *J. Jpn. Inst. Metals* **1983**, *47*, 683–687. [CrossRef] [PubMed]
47. Hu, F.X.; Shen, B.G.; Sun, J.R. Magnetic entropy change in $Ni_{51.5}Mn_{22.7}Ga_{25.8}$ alloy. *Appl. Phys. Lett.* **2000**, *76*, 3460–3462. [CrossRef]
48. Fukuda, T.; Maeda, H.; Yasui, M.; Kakeshita, T. Influence of magnetocrystalline anisotropy on martensitic transformation under magnetic field of single-crystalline Ni_2MnGa. *Scr. Mater.* **2009**, *60*, 261–263. [CrossRef]
49. Hu, F.X.; Sun, J.R.; Wu, G.H.; Shen, B.G. Magnetic entropy change involving martensitic transition in NiMn-based Heusler alloys. *J. Appl. Phys.* **2001**, *90*, 5216–5219. [CrossRef]
50. Hu, F.X.; Shen, B.G.; Sun, J.R.; Wu, G.H. Large magnetic entropy change in a Heusler alloy $Ni_{52.6}Mn_{23.1}Ga_{24.3}$ single cristal. *Phys. Rev. B.* **2001**, *64*, 132412. [CrossRef]
51. Mandal, K.; Pal, D.; Scheerbaum, N.; Lyubina, J.; Gutfleisch, O. Magnetocaloric effect in Ni–Mn–Ga alloys. *IEEE Trans. Magn.* **2008**, *44*, 2993–2996. [CrossRef]
52. Zhou, X.Z.; Li, W.; Kunkel, H.P.; Williams, G. Influence of the nature of the magnetic phase transition on the associated magnetocaloric effect in the Ni–Mn–Ga system. *J. Magn. Magn. Mater.* **2005**, *293*, 854–862. [CrossRef]
53. Zhou, X.Z.; Kunkel, H.; Williams, G.; Zhang, S.H.; Xue, D.H. Phase transitions and the magnetocaloric effect in Mn rich Ni–Mn–Ga Heusler alloys. *J. Magn. Magn. Mater.* **2006**, *305*, 372–376. [CrossRef]
54. Singh, S.; Esakki Muthu, S.; Senyshyn, A.; Rajput, P.; Suard, E.; Arumugam, S.; Barman, S.R. Inverse magnetocaloric effect in Mn_2NiGa and $Mn_{1.75}Ni_{1.25}Ga$ magnetic shape memory alloys. *Appl. Phys. Lett.* **2014**, *104*, 051905. [CrossRef]
55. Chatterjee, S.; Giri, S.; Majumdar, S.; De, S.K.; Koledov, V.V. Magnetic properties of full Heusler alloys $Ni_2MnGa_{1-x}Z_x$ with Z = Sn or Zn. *J. Magn. Magn. Mater.* **2012**, *324*, 1891–1896. [CrossRef]
56. Sasso, C.P.; Kuepferling, M.; Giudici, L.; Basso, V.; Pasquale, M. Direct measurements of the entropy change and its history dependence in Ni–Mn–Ga alloys. *J. Appl. Phys.* **2008**, *103*, 07B306. [CrossRef]
57. Khovaylo, V. Inconvenient magnetocaloric effect in ferromagnetic shape memory alloys. *J. Alloys Compd.* **2013**, *577*, S362–S366. [CrossRef]
58. Porcari, G.; Cugini, F.; Fabbrici, S.; Pernechele, C.; Albertini, F.; Buzzi, M.; Mangia, M.; Solzi, M. Convergence of direct and indirect methods in the magnetocaloric study of first order transformations: The case of Ni–Co–Mn–Ga Heusler alloys. *Phys. Rev. B* **2012**, *86*, 104432. [CrossRef]
59. Krenke, T.; Duman, E.; Acet, M.; Wassermann, E.F.; Moya, X.; Mañosa, L.; Planes, A. Inverse magnetocaloric effect in ferromagnetic Ni–Mn–Sn alloys. *Nat. Mater.* **2005**, *4*, 450–454. [CrossRef]
60. Han, Z.D.; Wang, D.H.; Zhang, C.L.; Tang, S.L.; Gu, B.X.; Du, Y.W. Large magnetic entropy changes in the $Ni_{45.4}Mn_{41.5}In_{13.1}$ ferromagnetic shape memory alloy. *Appl. Phys. Lett.* **2006**, *89*, 182507. [CrossRef]
61. Khan, M.; Ali, N.; Stadler, S. Inverse magnetocaloric effect in ferromagnetic $Ni_{50}Mn_{37+x}Sb_{13-x}$Heusler alloys. *J. Appl. Phys.* **2007**, *101*, 053919. [CrossRef]
62. Du, J.; Zheng, Q.; Ren, W.J.; Feng, W.J.; Liu, X.G.; Zhang, Z.D. Magnetocaloric effect and magnetic-field-induced shape recovery effect at room temperature in ferromagnetic Heusler alloy Ni–Mn–Sb. *J. Phys. D Appl. Phys.* **2007**, *40*, 5523–5526. [CrossRef]
63. Titov, I.; Acet, M.; Farle, M.; González-Alonso, D.; Mañosa, L.; Planes, A.; Krenke, T. Hysteresis effects in the inverse magnetocaloric effect in martensitic Ni–Mn–In and Ni–Mn–Sn. *J. Appl. Phys.* **2012**, *112*, 073914. [CrossRef]
64. Si, P.Z.; Liu, J.J.; Chen, C.Q.; Wu, Q.; Jiao, Z.W.; Ge, H.L. The effect of Ni-substitution on the magnetic properties of Ni_2MnGe Heusler alloys. *J. Alloys Compd.* **2008**, *462*, 1–3. [CrossRef]
65. Yu, H.J.; Fu, H.; Zeng, Z.M.; Sun, J.X.; Wang, Z.G.; Zhou, W.L.; Zua, X.T. Phase transformations and magnetocaloric effect in NiFeGa ferromagnetic shape memory alloy. *J. Alloys Compd.* **2009**, *477*, 732–735. [CrossRef]
66. Liu, J.; Scheerbaum, N.; Hinz, D.; Gutfleisch, O. A high-temperature coupling of martensitic and magnetic transformations and magnetic entropy change in Ni–Fe–Ga–Co alloys. *Scr. Mater.* **2008**, *59*, 1063–1066. [CrossRef]
67. Fu, H.; Yu, H.J.; Teng, B.H.; Zhang, X.Y.; Zu, X.T. Magnetic properties and magnetic entropy change of $Co_{50}Ni_{22}Ga_{28}$ alloy. *J. Alloys Compd.* **2009**, *474*, 595–597. [CrossRef]

68. Vivas, R.J.C.; Pedro, S.S.; Cruz, C.; Tedesco, J.C.G.; Coelho, A.A.; Carvalho, A.M.G.; Rocco, D.L.; Reis, M.S. Experimental evidences of enhanced magnetocaloric properties at room temperature and half-metallicity on Fe_2MnSi-based Heusler alloys. *Mater. Chem. Phys.* **2016**, *174*, 23–27. [CrossRef]
69. Murakami, Y.; Watanabe, Y.; Kachi, S. An X-ray Study of the Heusler-type Ordering in $AuAgZn_2$ Alloy. *Trans. Jpn. Inst. Met.* **1980**, *21*, 708–713. [CrossRef]
70. Muldawer, L. X-ray study of ternary ordering of the noble metals in $AgAuZn_2$ and $CuAuZn_2$. *J. Appl. Phys.* **1966**, *37*, 2062–2066. [CrossRef]
71. Ma, L.; Zhang, H.W.; Yu, S.Y.; Zhu, Z.Y.; Chen, J.L.; Wu, G.H.; Liu, H.Y.; Qu, J.P.; Li, Y.X. Magnetic-field-induced martensitic transformation in MnNiGa:Co alloys. *Appl. Phys. Lett.* **2008**, *92*, 032509. [CrossRef]
72. Kainuma, R.; Imano, Y.; Ito, W.; Morito, H.; Sutou, Y.; Oikawa, K.; Fujita, A.; Ishida, K.; Okamoto, S.; Kitakami, O.; et al. Metamagnetic shape memory effect in a Heusler-type $Ni_{43}Co_7Mn_{39}Sn_{11}$ polycrystalline alloy. *Appl. Phys. Lett.* **2006**, *88*, 192513. [CrossRef]
73. Zeng, Q.; Shen, J.; Zhang, H.; Chen, J.; Ding, B.; Xi, X.; Liu, E.; Wang, W.; Wu, G. Electronic behaviors during martensitic transformations in all-*d*-metal Heusler alloys. *J. Phys. Condens. Matter.* **2019**, *31*, 425401. [CrossRef]
74. Feng, L. Investigation on martensitic transformation and magnetic properties of all-*d*-metal Pd_2MnTi and Pt_2MnTi by first-principle calculations. *J. Supercond. Novel Magn.* **2020**, *33*, 2245–2250. [CrossRef]
75. Han, Y.; Wu, M.; Feng, Y.; Cheng, Z.; Lin, T.; Yang, T.; Wang, X. Competition between cubic and tetragonal phases in all-*d*-metal Heusler alloys, $X_{2-x}Mn_{1+x}V$ (X = Pd, Ni, Pt, Ag, Au, Ir, Co; x = 1, 0): A new potential direction of the Heusler family. *IUCrJ* **2019**, *6*, 465–472. [CrossRef] [PubMed]
76. Han, Y.; Wu, M.; Kuang, M.; Yang, T.; Chen, X.; Wang, X. All-*d*-metal equiatomic quaternary Heusler hypothetical alloys ZnCdTMn (T =Fe, Ru, Os, Rh, Ir, Ni, Pd, Pt): A first-principle investigation of electronic structures, magnetism, and possible martensitic transformations. *Results Phys.* **2018**, *11*, 1134–1141. [CrossRef]
77. Han, Y.; Bouhemadou, A.; Khenata, R.; Cheng, Z.; Yang, T.; Wang, X. Prediction of possible martensitic transformations in all-*d*-metal Zinc-based Heusler alloys from first-principles. *J. Magn. Magn. Mater.* **2019**, *471*, 49–55. [CrossRef]
78. Wang, X.; Wu, M.; Yang, T.; Khenata, R. Effect of Zn doping on phase transition and electronic structures of Heusler-type Pd_2Cr-based alloys: From normal to all-*d*-metal Heusler. *RSC Adv.* **2020**, *10*, 17829–17835. [CrossRef]
79. Yan, H.L.; Wang, L.D.; Liu, H.X.; Huang, X.M.; Jia, N.; Li, Z.B.; Yang, B.; Zhang, Y.D.; Esling, C.; Zhao, X.; et al. Giant elastocaloric effect and exceptional mechanical properties in an all-*d*-metal Ni-Mn-Ti alloy: Experimental and ab-initio studies. *Mater. Des.* **2019**, *184*, 108180. [CrossRef]
80. Shen, Y.; Sun, W.; Wei, Z.Y.; Shen, Q.; Zhang, Y.F.; Liu, J. Orientation dependent elastocaloric effect in directionally solidified Ni-Mn-Sn alloys. *Scr. Mater.* **2019**, *163*, 14–18. [CrossRef]
81. Wei, L.; Zhang, X.; Liu, J.; Geng, L. Orientation dependent cyclic stability of the elastocaloric effect in textured Ni-Mn-Ga alloys. *AIP Adv.* **2018**, *8*, 055312. [CrossRef]
82. Everhart, W.; Newkirk, J. Mechanical properties of Heusler alloys. *Heliyon* **2019**, *5*, e01578. [CrossRef]
83. Ozdemir Kart, S.; Cagin, T. Elastic properties of Ni_2MnGa from first-principles calculations. *J. Alloys Compd.* **2010**, *508*, 177–183. [CrossRef]
84. Agduk, S.; Gökoğlu, G. First-principles study of elastic and vibrational properties of Ni_2MnIn magnetic shape memory alloys. *Eur. Phys. J. B* **2011**, *79*, 509–514. [CrossRef]
85. Li, Y.; Huang, S.; Wang, W.; Liu, E.; Li, L. Ferromagnetic martensitic transformation and large magnetocaloric effect in $Ni_{35}Co_{15-x}Fe_xMn_{35}Ti_{15}$ (x = 2, 4, 6, 8) alloys. *J. Appl. Phys.* **2020**, *127*, 233907. [CrossRef]
86. Li, Y.; Qin, L.; Huang, S.; Li, L. Enhanced magnetocaloric performances and tunable martensitic transformation in $Ni_{35}Co_{15}Mn_{35-x}Fe_xTi_{15}$ all-*d*-metal Heusler alloys by chemical and physical pressures. *Sci. China Mater.* **2022**, *65*, 486. [CrossRef]
87. Aznar, A.; Gràcia-Condal, A.; Planes, A.; Lloveras, P.; Barrio, M.; Tamarit, J.; Xiong, W.; Cong, D.; Popescu, C.; Mañosa, L. Giant barocaloric effect in all-*d*-metal Heusler shape memory alloys. *Phys. Rev. Mater.* **2019**, *3*, 044406. [CrossRef]
88. Aznar, A.; Gràcia-Condal, A.; Planes, A.; Lloveras, P.; Barrio, M.; Tamarit, J.L.; Xiong, W.; Cong, D.; Popescu, C.; Mañosa, L. DFT investigation on the electronic, magnetic, mechanical properties and strain effects of the quaternary compound Cu_2FeSnS_4. *Crystals* **2020**, *10*, 509.
89. Taubel, A. Tailoring magnetocaloric effect in all-*d*-metal Ni-Co-Mn-Ti Heusler alloys: A combined experimental and theoretical study. *Acta Mater.* **2020**, *201*, 425. [CrossRef]
90. Li, G.; Liu, E.; Wu, G. *d-d* hybridization controlled large-volume-change martensitic phase transition in Ni-Mn-Ti based all-*d*-metal Heusler compounds. *J. Alloys Compd.* **2022**, *923*, 166369. [CrossRef]
91. Samanta, S.; Ghosh, S.; Chatterjee, M.K. Large magnetocaloric effect and magnetoresistance in Fe-Co doped $Ni_{50-x}(FeCo)_xMn_{37}Sn_{13}$ all-*d*-metal Heusler alloys. *J. Alloys Compd.* **2022**, *910*, 164929. [CrossRef]
92. Wu, M.; Zhou, F.; Khenato, R.; Kuang, M.; Wang, X. Phase transition and electronic studies of all-*d*-metal Heusler-type X_2nTi compounds (X = Pd, Pt, Ag, Au, Cu and Ni). *Front. Chem.* **2020**, *8*, 546947. [CrossRef]
93. Zhang, F.; Westra, K.; Shen, Q.; Batashev, I.; Kiecana, A.; van Dijk, N. The second-order magnetic phase transition and magnetocaloric effect in all-*d*-metal NiCoMnTi based Heusler alloy. *J. Alloys Compd.* **2022**, *906*, 164337. [CrossRef]

94. Jin, T.; Jung, Y. Classifying intermetallic tetragonal phase of all-*d*-metal Heusler alloys for catalysis applications. *Top. Catal.* **2022**, *65*, 208–214. [CrossRef]
95. Samanta, S.; Chatterjee, S.; Ghosh, S.; Mandal, K. Large reversible magnetocaloric effect and magnetoresistance by improving crystallographic compatibility condition in Ni(Co)-Mn-Ti all-*d*-metal Heusler alloys. *Phys. Rev. Mater.* **2022**, *6*, 094411. [CrossRef]

Disclaimer/Publisher's Note: The statements, opinions and data contained in all publications are solely those of the individual author(s) and contributor(s) and not of MDPI and/or the editor(s). MDPI and/or the editor(s) disclaim responsibility for any injury to people or property resulting from any ideas, methods, instructions or products referred to in the content.